31st Annual International Conference of the IEEE EMBS
Minneapolis, Minnesota, USA, September 2-6, 2009

Classification of Blood Regions in IVUS Images Using Three Dimensional Brushlet Expansions

Amin Katouzian, M. Alper Selver, Elsa D. Angelini, Bernhard Sturm, Andrew F. Laine

***Abstract*—The presence of non-coherent blood speckle patterns makes the assessment of lumen size in intravascular ultrasound (IVUS) images a challenging problem, especially for images acquired with recent high frequency transducers. In this paper, we present a robust three-dimensional (3D) feature extraction algorithm based on the expansion of IVUS cross-sectional images and pullback directions onto an orthonormal complex brushlet basis. Several features are selected from the projections of low-frequency 3D brushlet coefficients. These representations are used as inputs to a neural network that is trained to classify blood maps on IVUS images. We evaluated the algorithm performance using repeated randomized experiments on sub-samples to validate the quantification of the blood maps when compared to expert manual tracings of 258 frames collected from three patients. Our results demonstrate that the proposed features extracted in the brushlet domain capture well the non-coherent structures of blood speckle, enabling identification of blood pools and enhancement of the lumen area.**

I. Introduction

INTRAVASCULAR ultrasound (IVUS) is used clinically as a supplemental imaging modality to angiography in catheterization procedures, angioplasty or stent implantation, to screen the extent of atherosclerosis disease. Angiography provides a two-dimensional (2D) representation of 3D structures and depicts the sites of occlusions, while IVUS provides pathological as well as geometrical information about atherosclerotic plaques. During an interventional clinical procedure involving IVUS, hundreds of IVUS frames are acquired throughout each pullback within a coronary artery. Accurate information about lumen as well as arterial cross-sectional areas or isolation of plaques prior to tissue characterization requires a differentiation between blood and non-blood regions. This problem has motivated researchers to develop various techniques such as a 2D graph search in the Cartesian domain using 30 MHz transducer [1], 2D [2] and 3D [3] deformable models in the Cartesian domain using a 30 MHz transducer, 3D probability density functions (PDF)-based fast marching algorithm in the polar domain using a 20 MHz transducer [4], and a 2D statistical shape model-based approach in the polar domain using both 20 MHz and 40 MHz transducers [5].

Recently, high-frequency IVUS transducers such as the Volcano's (Rancho Cordova, CA) single-element mechanically rotating 45 MHz transducer were designed to provide grayscale images with improved spatial resolution. However, this makes the lumen border detection problem more challenging due to high scattering levels of blood speckle inside the lumen. In addition, intrinsic challenges associated with IVUS data such as the presence calcified plaques, bifurcations, guide wires, and more importantly motion of the catheter as well as the heart make existing algorithms only partially successful in clinical applications. As an alternative approach, several research teams have strived to detect blood regions or reduce blood noise effects in IVUS images, which could potentially be utilized as a pre-processing step for the detection of true lumen borders [6, 7]. The authors in [8] also presented a 3D supervised classification approach (one-class support vector machine) using three spatial, one temporal and three frequency-based features. They deployed three in-vivo datasets collected on swine using a 40MHz transducer, trained the classifier on thirty frames, and evaluated the algorithm for each dataset independently. The overall classification performance was reported as (97%, 82.3%, 2.8%) and (95.3%, 100%, 4%) for (sensitivity, specificity, support vector fraction) performance measures, on the two datasets. They further concluded that the highest performance was achieved using features dedicated to speckle.

In this paper, we present a framework for 3D feature extraction that expands IVUS volumes onto orthonormal directional brushlet basis functions. We select the 3D low-frequency complex brushlet coefficients to train a neural network to generate blood map images. We performed several experiments to identify the most informative features. Section 2 describes the data collection procedure. In section 3, we review brushlet analysis, feature extraction and specific classification methodologies. Experimental results and quantification analysis are provided in Section 4. Finally, we summarize and draw some conclusions on the study in Section 5.

Manuscript received April 23, 2009. This work was supported in part by Volcano Corporation (Rancho Cordova, CA).

A. Katouzian is with the Heffner Biomedical Imaging Lab in the Department of Biomedical Engineering of Columbia University, New York, NY USA, (phone: 212-854-5996, Fax: 212-854-5995, email: ak2432@columbia.edu).

M. A. Selver is with the Heffner Biomedical Imaging Lab in the Department of Electrical Engineering of Dokuz Eylül University, Izmir, Turkey, (email: as3675@columbia.edu).

E. D. Angelini is an Associate Professor of Computer Science Department at Telecom ParisTech, Paris, France, (email: elsa.angelini@telecom-paristech.fr).

B. Sturm is Senior Research Scientist at Volcano Corporation, Rancho Cordova, CA USA, (email: bsturm@volcanocorp.com).

A. F. Laine is Director of Heffner Biomedical Imaging Lab, Professor and Vice Chair of Department of Biomedical Engineering at Columbia University, New York, NY USA, (email: Laine@columbia.edu).

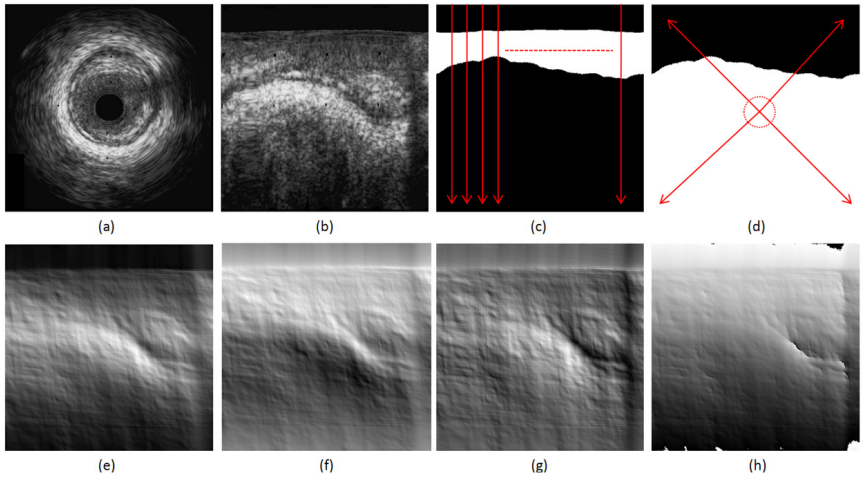

Fig. 1. IVUS frame in Cartesian (a) and polar (b) coordinates. Binary blood (c) and plaque (d) maps generated from manual tracing by an expert. The radial (c) and angular (d) distances are illustrated in red. Real part (e), imaginary part (f), magnitude (g) and phase (h) of brushlet coefficients computed on the radial image (b) along a single orientation.

II. *In-Vivo* Data Collection

We collected IVUS grayscale images using a single-element mechanically rotating 45 MHz Revolution™ transducer and a s5™ imaging system manufactured by Volcano Corporation (Rancho Cordova, CA, USA). The catheter was advanced on top of a guide wire from the femoral artery toward the site of coronary arterial occlusion (i.e. right coronary artery (RCA), left anterior descending (LAD) artery, or left circumflex (LCX) artery) via the aorta. During image acquisition, the catheter was pulled back from distal to proximal locations with a speed of 0.5mm/sec or 1.0mm/sec, acquiring 30 frames/sec. The original images, acquired in polar coordinates (as illustrated in Figure 1), are then mapped to Cartesian coordinates to construct typical IVUS images.

III. Methods

Unlike IVUS images acquired with 20 MHz 64-element transducers, the 2D detection of the lumen contour can be extremely challenging in IVUS images acquired with 45 MHz transducers. Therefore, interventional radiologists typically go back and forth over consecutive frames to be able to visually locate the lumen contour on a single frame. By doing so, blood speckle and plaques embody respectively random and coherent spatial patterns, suggesting that 3D processing may be required to differentiate these elements. This motivated us to develop a 3D brushlet classification algorithm to differentiate between blood speckle and non-blood regions in IVUS images.

A. *Brushlet Analysis*

Brushlet basis were first introduced in [9], as a family of steerable functions, that provide projected coefficients associated with particular brushstrokes (of specific sizes and orientations) yielding the characterization of textural features with distinct directions corresponding to specific brushlet functions. The functions divide the real axis into subintervals $[a_n, a_{n+1}]$ of length l_n, and define a brushlet analysis function as follows:

$$u_{j,n}(x) = b_n\left(x - {l_n}/{2}\right)e_{j,n}(x) + v(x-a_n)e_{j,n}(2a_n - x) - v(x-a_{n+1})e_{j,n}(2a_{n+1} - x) \quad (1)$$

The b_n and v are two localized window functions providing the orthogonality property. The complex orthonormal basis function $u_{j,n}$, can be constructed using these two functions along with the complex exponential function $e_{j,n}$ that is defined as:

$$e_{j,n}(x) = \frac{1}{\sqrt{l_n}} e^{-2i\pi j\frac{(x-a_n)}{l_n}} \quad (2)$$

Given any one-dimensional signal f in $L^2(R)$, its Fourier transform $\hat{f}$ can be projected onto the brushlet basis as:

$$\hat{f} = \sum_n \sum_j \hat{f}_{n,j} u_{n,j} \quad (3)$$

where $\hat{f}_{n,j}$ are the brushlet coefficients. It has been shown that the projected of $\hat{f}$ onto the brushlet basis can be implemented in an efficient fashion using a folding technique and fast Fourier transform (FFT) [10]. In this work, we projected 3D IVUS volumes in polar coordinates with brushlet overcomplete expansion [11]. Figures 1(a) and (b) illustrate a single IVUS slice in both Cartesian and polar coordinates and its corresponding brushlet coefficients, along a single orientation. Binary masks based on manually traced vessel wall and lumen contours by an expert, are also illustrate in this figure.

B. *Feature Extraction*

One of the main advantages of a brushlet expansion is that one can select features along specific directions. This can be reliably performed by tilling the Fourier domain into quadrants (sub-cubes), each representing a specific size and orientation of a "brushstroke." In order to train and then use a classifier to extract the blood regions on IVUS images, we built a vector of features, combining *image information*, via brushlet expansion, and *geometric constraints*. First, for each quadrant of brushlet coefficients, we combined redundant coefficient value information:

Table 1. Classification results using neural networks with different topologies: N-M-1; N and M are the number of neurons in the input and hidden layers, respectively. Also shown are results using different numbers of features. Correct classification (CC) rate, sensitivity (SE), specificity (SP) and correct segmentation (S) rate are reported. The better results are highlighted in yellow. The best performance was achieved using 34 features (N) and network topology of N-34-1 (green).

Neural Network Topology (N-M-1)	N=32 Features				N=33 Features				N=34 Features			
	CC	SE	SP	S	CC	SE	SP	S	CC	SE	SP	S
N-3-1	93.31	81.47	92.55	**70.21**	93.67	83.16	93.02	**71.22**	94.11	83.42	95.90	**71.34**
N-5-1	94.15	87.69	95.86	**71.66**	93.82	84.08	95.98	**72.27**	94.56	83.10	96.90	**72.21**
N-10-1	94.51	86.65	97.14	**74.31**	94.32	85.83	97.04	**75.47**	94.69	86.75	96.56	**76.94**
N-15-1	94.85	87.47	96.68	**75.20**	94.86	78.46	97.10	**76.41**	95.04	87.88	97.82	**78.56**
N-20-1	94.27	86.61	96.80	**75.07**	94.82	77.08	97.98	**78.05**	95.10	88.20	97.14	**78.27**
N-34-1	95.12	86.73	96.38	**77.23**	95.33	77.32	98.10	**77.94**	95.84	86.80	97.87	**79.59**

(1) magnitude values, which are typically used in spectral-based tissue characterization algorithms [12-14], (2) phase values, (3) real and (4) imaginary values.

Indeed, in preliminary experiments, we observed significant improvement of the classifier performance when using redundant coefficient information versus only (real, imaginary) or (magnitude, phase) information.

Geometric constraints were defined using two distance maps: a radial *distance map*, with respect to the transducer surface, computed in polar coordinates (to encode the fact that the blood pool is close to the transducer), and a direct map of individual pixel locations, to encode geometric information in the feature vector, which is built via an arbitrary rasterization of the IVUS data. These two geometric constraints are illustrated in Figure 1.

C. *Classification*

Feature vectors are used as the input of a neural network classifier. More specifically, we employed a Multi Layer Perceptron (MLP) [16], which was trained using Back Propagation (BP) algorithm with adaptive learning rate. The specifications of the MLP design are further explained in the next section.

IV. Experimental Results

We deployed 258 IVUS frames in pullbacks data collected from three patients, consisting of small, medium and large blood pools to accommodate for diversity within patients. For each pullback, the volumetric IVUS data was partitioned into sub-volumes of size $(512\times512\times8)$. An overcomplete expansion was performed through tiling of the Fourier domain into four, four and two sub-cubes in x, y and pullback direction that provided adequate spatial-temporal resolution. We only preserved the [2×2×2] low-frequency redundant coefficients, leading to a total of N=32 coefficients-based features. Finally, by including the two geometric features, we constructed our feature vector with N=34 features. For the sake of simplicity and to enable a fair comparison, we used, in our initial experiments, an MLP topology as previously employed in IVUS related studies for lumen border detection [2] and catheter motion compensation [15]. The MLP had one hidden layer and one neuron as output with linear activation functions. The network goal, adaptive learning rate, and maximum number of iterations set to 0.001, 0.01, and 5000 epochs, respectively. For each experiment, the training set was constructed with random selection of 2/3 of the dataset (172 frames) and the remaining 1/3 (86 frames) were used for testing. For this purpose, binary masks for blood and non-blood regions in each frame were generated using manually traced lumen borders by an expert, as illustrated in Figure 1(b) and (c).

First, we repeated the experiments with different numbers of neurons in the hidden layer (20 experiments for each) to find out the optimal setting. In order to evaluate the classification accuracy, the correct classification (CC) and segmentation (S) rates were defined as (TN+TP)/(TN+TP+FP+FN) and (TP)/(TP+FP+FN), respectively, where TP, TN, FP, and FN correspond to true positive, true negative, false positive, and false negative rates. We computed the S value, in addition to traditional CC rate, for fair representation of classification results since the lumen embodied small area compared to the whole IVUS image, causing large TN rates. The sensitivity (SE) and specificity (SP) rates were also defined as TP/(TP+FN) and TN/(TN+FP), respectively. Table 1 summarizes the results and demonstrates that a hidden layer with more than 15 neurons does not alter the results significantly. The best performance was achieved when both geometric features were used, confirming the influence of such features. We constructed blood maps using the output of linear activation functions and represented the least (blue) as well as the most (red) probable blood regions in color jet spectrum. Figure 2 illustrates a blood map generated by the neural network and corresponding to a relatively small vessel. The constructed blood map provided fair representation of the lumen cavity, confirming that the extracted features were sufficiently reliable.

Although blood maps offer necessary information on blood regions they are not sufficient for detection of the lumen border, which is a priority for any blood detection algorithm. For this purpose, we used the output of the linear activation function in the last neuron layer of the neural network and constructed 8-bit grayscale images by mapping these values from the range of [0,1] onto [0,255], linearly. Subsequently, we used thresholding followed by edge detection to delineate the lumen border. Although the value of 0.5 (128 in grayscale) seemed to be the appropriate threshold, we experimented with several values to validate this setting. Results are listed in Table 2. Given a threshold value of 0.5, the classifier slightly overestimated the blood region compared with a threshold value of 0.45. This can be due to the non-linear behavior of the neural network or insufficiency of our current training dataset.

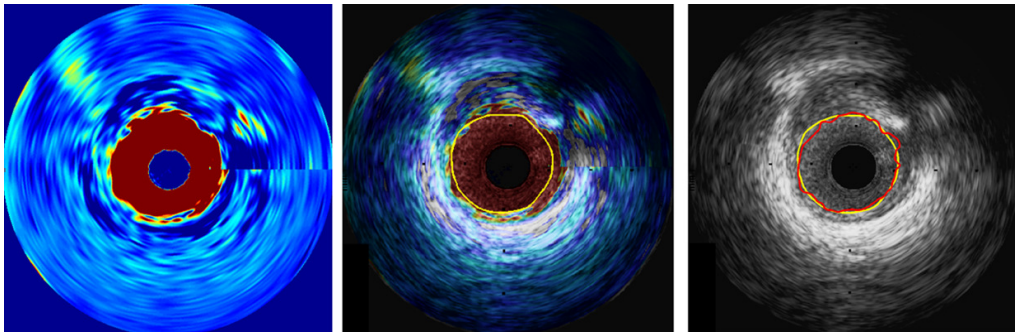

Fig. 2. Generated blood map (left), superimposed blood map on original grayscale IVUS image (middle) with manually traced lumen border (yellow), and automated detected lumen border (red) by thresholding output values of a neural network.

Table 2. Classification results and comparison between manual and optimal automated lumen border, generated from a thresholded blood map with an optimized threshold value through linear regression analysis and computation of Tanimoto Coefficients (η). The best performance was achieved using threshold value of 0.45 (green).

Threshold value	Classification Statistics Case 1, Case 2, Case 3						Comparison Between Manually Traced and Automated Detected Borders									
							Case 1					Case 2				
	CC	FP	FN	SE	SP	S	η_{ave}	η_{max}	η_{min}	η_{std}	Correlation (p<0.0001)	η_{ave}	η_{max}	η_{min}	η_{std}	Correlation (p<0.0001)
0.25	94.42	5.10	4.13	95.86	94.10	75.87	73.97	84.91	65.11	4.97	0.82	76.81	86.97	61.46	5.93	0.85
0.35	95.50	3.38	6.94	93.06	96.05	79.09	78.20	88.97	60.07	6.24	0.82	76.85	89.49	59.62	7.21	0.82
0.4	95.75	2.76	8.75	91.25	96.76	79.71	79.29	88.03	71.05	4.43	0.88	76.60	89.64	58.61	7.41	0.76
0.45	95.86	2.25	10.83	89.17	97.36	79.77	79.94	87.70	74.76	3.97	0.86	76.52	91.37	57.43	7.73	0.75
0.5	95.84	1.81	13.19	86.80	97.87	79.59	78.59	87.80	71.71	4.23	0.88	76.24	90.39	56.11	8.24	0.66
0.55	95.68	1.45	16.07	83.93	93.31	78.02	76.54	88.94	69.81	4.67	0.88	75.50	89.01	54.85	8.58	0.67
0.6	95.39	1.13	19.3	80.70	97.68	76.20	74.23	86.03	68.18	4.27	0.91	73.98	87.51	53.12	8.77	0.63
0.65	94.97	0.87	23.02	76.98	98.99	73.66	71.59	81.42	63.41	4.45	0.93	72.60	86.78	51.93	9.29	0.58
0.75	93.61	0.45	32.59	67.40	99.47	65.87	63.70	72.34	56.76	4.00	0.95	67.64	84.58	48.44	10.07	0.54

V. Discussion and Conclusion

In this paper we presented a 3D blood detection algorithm on IVUS images acquired with a 45MHz single element Revolution™ (Volcano Corporation) transducer. We expanded IVUS volumes onto brushlet basis functions in an overcomplete fashion. We extracted brushlet-based features from quadrants corresponding to low frequency components, combined them with geometric features and used a neural network as a classifier. The reconstructed blood maps were compared to blood pools quantified with manually traced lumen borders, confirming that the proposed features were sufficiently representative of blood speckle appearance and localization. We also extracted the lumen border based on reconstructed grayscale images masked with the output of the neural network. We plan to combine the proposed features along with contrast, homogeneity information to achieve more robust results. We also plan to train the classifier using a more diverse dataset and deploy a support vector machine (SVM) classifier as an alternative to neural network.

References

[1] M. Sonka, X. Zhang, M. Siebes, M. S. Bissing, S. C. DeJong, S. M. Collins, C. R. McKay, "Segmentation of Intravascular Ultrasound Images: A Knowledge-Based Approach," IEEE Trans. Med. Imag. Vol. 14, No. 4, pp. 719-732, 1995.

[2] M. Plissiti, D. Fotidadis, L. Michalis, G. Bozios, "An Automated Methos for Lumen and Media-Adventitia Border Detection in a sequence of IVUS frames," IEEE Trans. Info. Tech. Biomed., Vol. 19, No. 10, pp. 996-1011, 2000.

[3] R. Shekhar, R. M. Cothren, D. G. Vince, S. Chandra, J. D. Thomas, J. F. Cornhill, "Three-Dimensional Segmentation of Luminal and Adventitial Borders is Serial Intravascular Ultrasound Images," Computerized Med. Imag. and Graphics, vol. 23, pp. 299-309, 1999.

[4] M. R. Cardinal, J. Meunier, G. Soulez, R. L. Maurice, E. Therasse, G. Cloutier, "Intravascular Ultrasound Image Segmentation: A Three-Dimensional Fast-Marching Method Based on Gray Level Distribution," IEEE. Trans. Med. Imag., Vol. 25, No. 5, pp. 590-601, 2006.

[5] G. Unal, S. Bucher, S. Carlier, G. Slabaugh, T. Fang, K. Tanaka, "Shape-Driven Segmentation of the Arterial Wall in Intravascular Ultrasound Images," IEEE Trans. Info. Tech. Biomed., Vol. 12, No. 3, pp. 335-347, 2008.

[6] D. Rotger, P. Radeva, E. F. Nofrerias, J. Mauri, "Blood Detection in IVUS Images for 3D Volume of Lumen Changes Measurement Due to Different Drugs Administration," CAIP 2007, LNCS 4673, pp. 285-292.

[7] K. Hibi, A. Takagi, X. Zhang, T. T. Teo, H. N. Boneau, P. G. Yock, P. J. Fitzgerald, "Feasibility of a Novel Blood Reduction Algorithm to Enhance Reproducibility of Ultra-High-Frequency Intravascular Ultrasound Images," Circulation, Vol. 102, No. 14, pp. 1657-1663, 2000.

[8] S. M. O'Malley, M. Naghavi, I. A. Kakadiaris, "One-Class Acoustic Characterization Applied to Blood Detection in IVUS," MICCAI 2007, Part I, LNCS 4791, pp. 202-209.

[9] F. Meyer and R. R. Coifman, "Brushlets: A tool for directional image analysis and image compression," Applied and computational harmonic analysis, vol. 4, pp. 147-187, 1997.

[10] P. Ausher, G. Weiss, M. V. Wickerhauser, "Local sine and cosine bases of Coifman and Meyer and the construction of smooth wavelets," in Wavelets- A tutorial in Theory and Application, vol. 2, Wavelet Analysis and its Applications, C. K. Chui, Ed. San Diego: Academic Press, 1992, pp. 237-256.

[11] E. Angelini, A. Laine, S. Takuma, J. Holmes, S. Homma, "LV Volume Quantification via Spatio-Temporal Analysis of Real-Time 3D Echocardiography," IEEE Trans. Med. Imag., Vol. 20, No. 6, pp. 457-469, 2001.

[12] A. Nair, B. D. Kuban, M. Tuzcu, P. Schoenhagen, S. E. Nissen, D. G. Vince, "Coronary Plaque Classification With Intravascular Ultrasound Radiofrequency Data Analysis," Circulation, vol. 106, no. 17, pp. 2200-2206, 2002.

[13] A. Katouzian, S. Sathyanarayana, B. Baseri, E. Konofagou, S. G. Carlier, "Challenges in Atherosclerotic Plaque Characterization with Intravascular Ultrasound (IVUS): From Data Collection to Classification," IEEE Trans. Info. Tech. Biomed., Vol. 12, No. 3, pp. 315-327, 2008.

[14] M. Kawasaki, H. Takatsu, T. Noda, K. Sano, Y. Ito, K. Hayakawa, K. Tsuchiya, M. Arai, K. Nishigaki, G. Takemura,S. Minatoguchi,T. Fujiwara, H. Fujiwara," In Vivo Quantitative Tissue Characterization of Human Coronary Arterial Plaques by Use of Integrated Backscatter Intravascular Ultrasound and Comparison With Angioscopic Findings," Circulation, pp. 2487- 2492, 2002.

[15] M. Rosales, P. Radeva, O. R. Leor, D. Gil, "Modeling of image-catheter motion for 3-D IVUS," Medi. Imag. Anal., Vol. 13, No. 1, pp. 91-104, 2009.

[16] S. Haykin, Neural Networks: A Comprehensive Foundation. Upper Saddle River, NJ: Prentice Hall, 1998.